High-resolution FTIR spectroscopy of chlorodifluoromethane: ν2 and ν7

ARTICLE *in* CHEMICAL PHYSICS · JUNE 2002

Impact Factor: 1.65 · DOI: 10.1016/S0301-0104(02)00454-8

3 AUTHORS, INCLUDING:

Evan G Robertson
La Trobe University
95 PUBLICATIONS **1,781** CITATIONS

ELSEVIER

Chemical Physics 279 (2002) 239–248

Chemical Physics

www.elsevier.com/locate/chemphys

High-resolution FTIR spectroscopy of chlorodifluoromethane: v_2 and v_7

Christopher D. Thompson, Evan G. Robertson *, Don McNaughton

School of Chemistry, P.O. Box 23, Monash University, Vic. 3800, Australia

Received 2 January 2002

Abstract

High-resolution FTIR spectra of chlorodifluoromethane (R22) were measured both at room temperature and cooled to approximately −100 °C in a collisional cooling cell. A rovibrational analysis was performed for v_2, the a/c-hybrid band at 1313 cm^{-1} and v_7, the b-type band at 1351 cm^{-1}. 7400 and 1700 lines were assigned to $CH^{35}ClF_2$ and $CH^{37}ClF_2$, respectively, with quantum numbers up to $J = 98$ and $K_a = 46$. Effective constants to the sextic level have been fitted using Watson's A-reduction Hamiltonian. More accurate spectroscopic constants were obtained by fitting the two states simultaneously, taking into account both first- and second-order *c*-axis Coriolis interactions between the two bands. The v_2 band is predominantly a-type, but weaker c-type transitions assigned for $CH^{35}ClF_2$ enable the a/c-hybrid character (μ_a^2/μ_c^2) to be determined as 5.76.

Keywords: IR spectroscopy; Chlorodifluoromethane; Hydrochlorofluorocarbons; Rovibrational analysis; Collisional cooling

1. Introduction

The Montreal Protocol specifies that use of the refrigerant chlorodifluoromethane (R22) is to be incrementally phased out by the year 2020 [1]. Despite this, R22 has surfaced as one of the prime replacement gases for the ozone depleting Freons R11 (CCl_3F) and R12 (CCl_2F_2). Itself an ozone depleting species (ODP = 0.055) and a greenhouse gas (global warming potential = 1700) [2], R22 has a tropospheric lifetime of 15–20 years [3], and consequently concentrations of the gas have increased considerably. The infrared absorption cross-section of the R22 spectrum is currently used for the determination of atmospheric concentrations of the species. The importance of this molecule has lead to a focussed effort in assigning the high-resolution infrared structure of all the infrared bands.

Analysis of the pure rotational spectrum has extended from the centimetre wave region into the far infrared [4–6] and the most up-to-date data set provided by Kisiel et al. [7] includes ground state constants to the sextic level for three isotopomers, $CH^{35}ClF_2$, $CH^{37}ClF_2$ and $^{13}CH^{35}ClF_2$. The anharmonic force field of the molecule has also been

* Corresponding author. Tel.: +61-3-9905-4566; fax: +61-3-9905-4597.

E-mail address: evan.robertson@sci.monash.edu.au (E.G. Robertson).

0301-0104/02/$ - see front matter
PII: S0301-0104(02)00454-8

calculated recently using ab initio force field parameters which were scaled to agree with experimental data to a high level of accuracy. This included both the vibration–rotation interaction constants (α) and the polarisation ratios for the a/c-type bends in the spectrum [8].

The following work completes the global rovibrational analysis of the fundamental bands of $CH^{35}ClF_2$ which lie in the range 300–3050 cm^{-1}. The molecule has C_s symmetry and its nine infrared active bands in the spectrum are either a/c-type $(\nu_1 - \nu_6)$ or b-type $(\nu_7 - \nu_9)$, the corresponding upper states belonging to the A′ and A″ representations, respectively. Until this work, only seven of these bands have been characterised through high-resolution studies. Previously, rotational constants have been determined for the ν_1 band of $CH^{35}ClF_2$ and $CH^{37}ClF_2$ at 3022 cm^{-1} [9], the Coriolis coupled doublet ν_3 (1109 cm^{-1}) and ν_8 (1128 cm^{-1}) of $CH^{35}ClF_2$ [10], the ν_4 state at 809.3 cm^{-1} and its Fermi resonance with the overtone $2\nu_6$ at 829.0 cm^{-1} for $CH^{35}ClF_2$ [11], the ν_5 state at 596.4 cm^{-1} for $CH^{35}ClF_2$, [12,13], and another Coriolis coupled doublet of ν_6 at 366 cm^{-1} and ν_9 at 413 cm^{-1} complete for both $CH^{35}ClF_2$ and $CH^{37}ClF_2$ [6,14]. The two vibrational states analysed in this work are the a/c-type band ν_2 at 1313 cm^{-1} and the b-type band ν_7 at 1351 cm^{-1} corresponding to the –CH bends in the HCCl plane and perpendicular to it.

2. Experimental

This work is some of the first conducted using a recently developed enclosive flow collisional cooling cell, based on a design by Bauerecker [15], which is described in further detail in a separate paper [16]. Briefly, it consists of a porous cylindrical colander with a window at one end and a mirror at the other, allowing a double optical pass with total OPL ~140 cm. Buffer gas, precooled by passing through a liquid N_2 jacket, enters through the pores and is continually pumped via an outlet

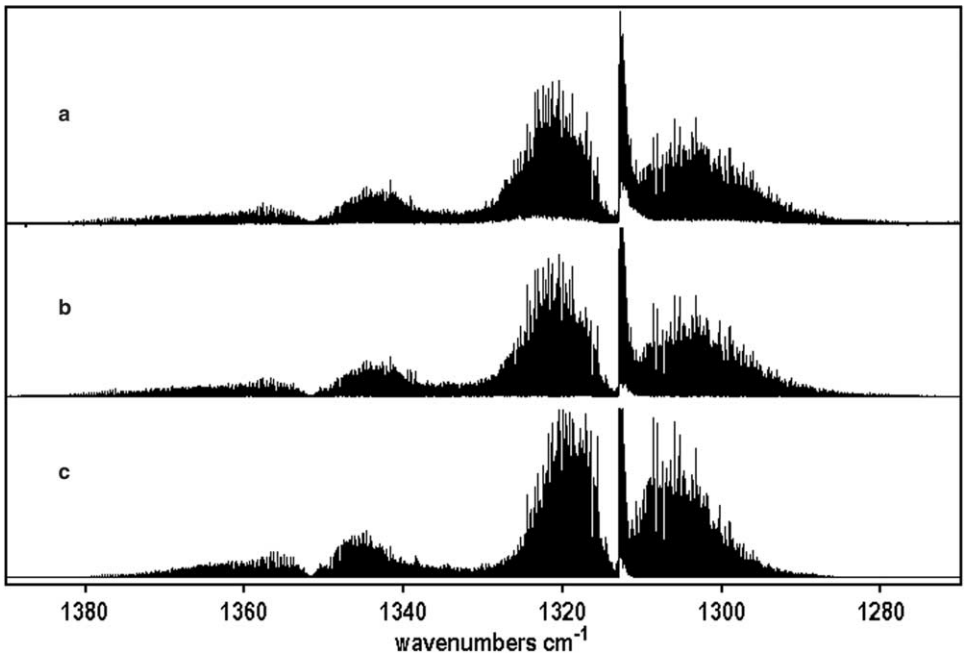

Fig. 1. FTIR spectra of $CHClF_2$ ν_2/ν_7 at room temperature (a) and cooled (b). (c) Simulation using constants from Tables 2 and 4, $T_{rot} = 180$ K and FWHH Gaussian linewidth 0.0025 cm^{-1}.

port near the mirror. An inlet tube, which is heatable to prevent frozen sample, serves to introduce the sample gas into the flow of the cold buffer gas.

R22 was measured using a commercial sample (BOC gases) with isotopomers in ratios of natural abundance without further purification. Internal temperatures varied from 120–200 K with the sample nozzle heated to approximately 210 K. Equilibrium cell pressures ranged from 1.0–2.5 Torr. Spectra were also measured using the cell in a static fashion without buffer gas or coolant. High-resolution spectra were measured at nominal resolution 0.0019 cm^{-1} using a Bruker HR120 FTIR spectrometer with a Globar source and a liquid nitrogen cooled HgCdTe detector. Data was collected over a range limited by the CaF_2 cell window (>900 cm^{-1}) and a 1500 cm^{-1} high-pass filter.

3. Results

A high resolution, room temperature spectrum of $CHClF_2$ in the region of ν_2 and ν_7 is shown in Fig. 1(a). The density of lines is considerable, and there is some overlap between the two bands. Cooler spectra, such as that in Fig. 1(b), show fewer lines and less overlap and were therefore examined first in the rovibrational analyses.

3.1. $CH^{35}ClF_2$

To aid the initial assignment process, spectra were simulated using a rigid rotor Hamiltonian. The ground state rotational constants are known [5], and the upper state constants were computed using vibration–rotation interaction constants α predicted from the anharmonic force field of Palmieri et al. [8]. Peak lists were examined using

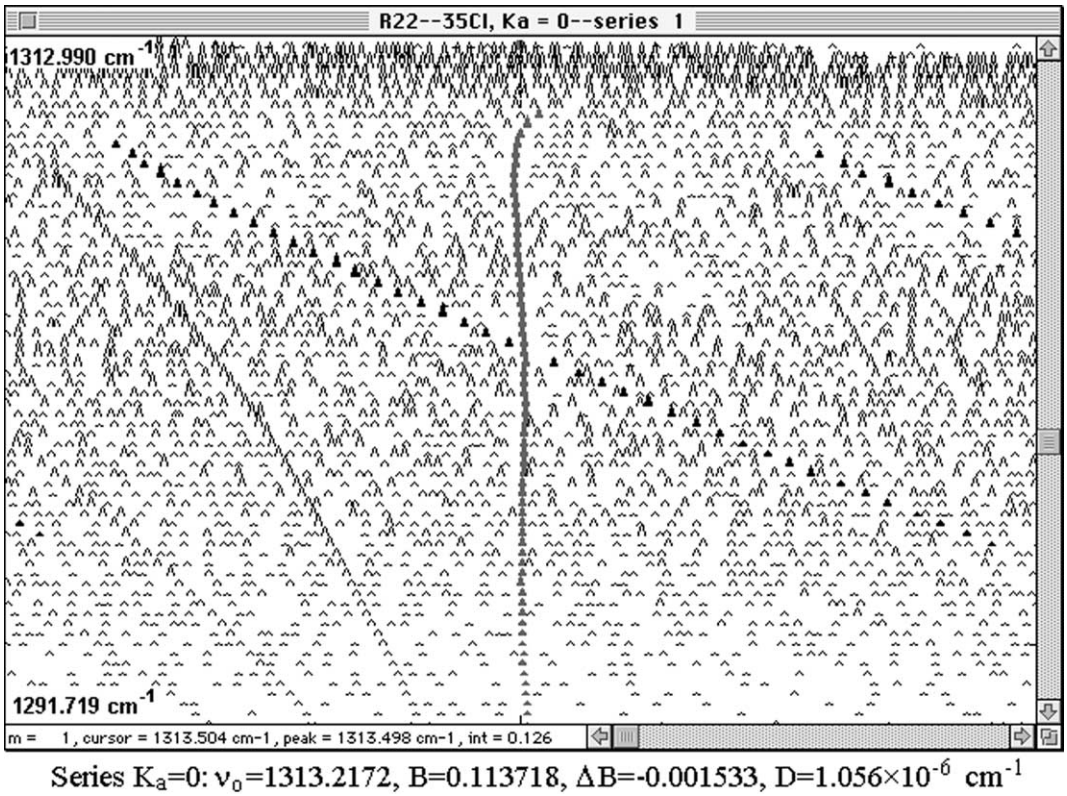

Fig. 2. Loomis–Wood plot showing the $^qP_0$ series of $CH^{35}ClF_2$ in the centre. The positions of the selected peaks are fitted to a third-order polynomial and the centre of each horizontal strip is adjusted accordingly. The analogous series of $CH^{37}ClF_2$ is also highlighted.

an interactive program Macloomis, which displays a spectrum in Loomis–Wood (Fortrat) format [17]. Although designed to identify related transitions in linear molecules, it succeeds with asymmetric tops when the line spacing is sufficiently regular. Fig. 2 shows a portion of the v_2 band with the $^{q}P_0$ series selected in a Macloomis plot. The peak positions are fitted to a third-order polynomial and the centre of each horizontal strip is adjusted accordingly. Commencing with the most abundant $CH^{35}ClF_2$ isotopomer, approximately 2500 a-type ^{q}R and ^{q}P transitions of v_2 and 2000 b-type $^{r}R/^{p}R$ and $^{p}P/^{r}P$ lines of v_7 were assigned in this fashion, with $J \leqslant 70$ and $K_a \leqslant 34$. Examination of the room temperature spectra of v_2 and v_7 and assignment of further lines extended the number and range of assigned transitions, yielding a total of 4622 ($J \leqslant 98$, $K_a \leqslant 46$) and 2874 ($J \leqslant 72$, $K_a \leqslant 45$) lines, respectively. In addition to the a-type lines that dominate the v_2 band, weaker c-type transitions of high K_a were detected at the outskirts of the rotational envelope in the warmer spectrum, and 448 ^{p}P lines were assigned.

The data were fitted to Watson's A-reduced Hamiltonian using the program SPFIT written by Pickett [18]. Initially and for assignment purposes, both bands were fitted individually without consideration of any interaction between them. Transitions were given an experimental uncertainty of 0.0004 cm^{-1} (approximately 15% of the effective linewidth). Unresolved transitions with a separation calculated to lie in the range 0.0008–0.0020 cm^{-1} were omitted. To achieve a satisfactory fit, centrifugal distortion constants up to the sextic level were all freely varied, and the results are given in Table 1. The rms deviations of 0.00116 and 0.00032 cm^{-1} for v_2 and v_7 data, respectively, reflect the range of J and K_a quantum numbers fitted in each case. In both cases the quartic and sextic constants differed from their ground state values considerably, by up to three orders of magnitude. Moreover, those parameters from v_2 consistently displayed a shift of nearly equal magnitude but opposite direction to those of the corresponding v_7 parameters. The upper state C rotational constants exhibit a similar pattern of

Table 1
Effective rotational constants in Watson's A-reduced Hamiltonian for v_2 and v_7 states of $CH^{35}ClF_2$ (cm^{-1})

Constant	Ground state[a]	v_2	v_7
Band centre	–	1313.093632 (24)[b]	1351.701955 (34)
A	0.3413929510	0.34094310 (18)	0.3410689 (2)
B	0.1621539520	0.16202701 (9)	0.1620690 (2)
C	0.1169955380	0.11563804 (3)	0.1182825 (1)
$\Delta_J \times 10^{-6}$	0.0522494799	0.031152 (34)	0.075231 (117)
$\Delta_{JK} \times 10^{-6}$	0.1531526186	0.278824 (200)	0.017937 (417)
$\Delta_K \times 10^{-6}$	0.1641635695	0.071565 (232)	0.275061 (413)
$\delta_J \times 10^{-6}$	0.0147462015	0.023808 (18)	0.004376 (64)
$\delta_K \times 10^{-6}$	0.1672757225	0.112701 (171)	0.232580 (622)
$\Phi_J \times 10^{-12}$	0.02334949	−0.774 (7)	1.455 (42)
$\Phi_{JK} \times 10^{-12}$	0.33689974	7.711 (50)	−10.389 (198)
$\Phi_{KJ} \times 10^{-12}$	−0.0433633	−16.924 (152)	21.002 (785)
$\Phi_K \times 10^{-12}$	0.10674051	13.426 (125)	−11.644 (618)
$\phi_J \times 10^{-12}$	0.01087419	0.180 (4)	−0.142 (21)
$\phi_{JK} \times 10^{-12}$	0.18346025	−2.822 (48)	6.981 (254)
$\phi_K \times 10^{-12}$	3.06545403	1.592 (235)	12.092 (1862)
J_{max}	–	98	72
$K_{a\ max}$	–	46	45
Number trans.	–	4622	2874
rms deviation (cm^{-1})	–	0.00116	0.00032
σ_{dev}	–	2.902	0.811

[a] Ground state constants from [6].
[b] Figures in brackets are one S.D. according to the least squares fit in units of the least significant figure quoted.

shifts. Such behaviour is characteristic of states coupled by of a *c*-axis Coriolis interaction.

A global fit of the v_2/v_7 bands was performed with inclusion of a first-order term ξ^c, leading to far more reasonable distortion constants. The resultant value for the Coriolis constant ($\xi^c = 0.239$), was unrealistic however as it relates via the equation:

$$\xi^c = C\zeta^c\{(\omega_2/\omega_7)^{1/2} + (\omega_7/\omega_2)^{1/2}\}$$

to a value of $\zeta^c = 1.022$ which is greater than 1, the upper limit for ζ. Inclusion of a second-order Coriolis term (η^{ab}) both further improved the quality of the fit and gave reasonable values of $\xi^c = 0.2275$ cm^{-1} (corresponding to $\zeta^c = 0.971$) and $\eta^{ab} = -1.10 \times 10^{-4}$ cm^{-1}. The v_2 and v_7 sextic centrifugal distortion constants were constrained to ground state values since allowing them to vary resulted in constants that were not well determined, changed very little in the fitting procedure, and made no appreciable difference to an already high quality fit. The decision to constrain the sextic constants in the Coriolis fits was made for two reasons. Firstly, several of the constants were found to have large uncertainty, despite the ample number of assigned transitions. Secondly, while the other constants converged to a stable value, their inclusion made little difference to a fit which already agreed well with the predicted line uncertainty. The high accuracy of simulations of the high-resolution spectra also suggested the fitting of these constants was unnecessary. Molecular parameters from the global Coriolis fit are summarized in Table 2. The rms error is just 0.00043 cm^{-1}, and notably the inclusion of the *c*-axis Coriolis terms results in upper state quartic centrifugal distortion constants that lie within just 3% of the ground state values.

It should be noted that as the molecule has C_s symmetry an *a*-axis Coriolis interaction is also possible between the two states. Inclusion of the parameter ξ^a lead to a poorly determined value

Table 2
Rotational constants in Watson's A-reduced Hamiltonian for v_2 and v_7 states of $CH^{35}ClF_2$ incorporating a *c*-axis Coriolis interaction

Constant	Ground state[a]	v_2	v_7
Band centre	–	1313.095198 (19)[b]	1351.701708 (24)
A	0.3413929510	0.3409425 (1)	0.3410776 (1)
B	0.1621539520	0.1620259 (1)	0.1620598 (1)
C	0.1169955380	0.1169684 (155)	0.1169448 (155)
$\Delta_J \times 10^{-6}$	0.0522494799	0.051711 (10)	0.052820 (30)
$\Delta_{JK} \times 10^{-6}$	0.1531526186	0.151971 (366)	0.154790 (476)
$\Delta_K \times 10^{-6}$	0.1641635695	0.167201 (344)	0.160460 (435)
$\delta_J \times 10^{-6}$	0.0147462015	0.015060 (7)	0.014387 (16)
$\delta_K \times 10^{-6}$	0.1672757225	0.168620 (185)	0.165401 (185)
$\Phi_J \times 10^{-12}$	0.02334949	0.02334949[c]	0.02334949[c]
$\Phi_{JK} \times 10^{-12}$	0.33689974	0.33689974[c]	0.33689974[c]
$\Phi_{KJ} \times 10^{-12}$	−0.0433633	−0.0433633[c]	−0.0433633[c]
$\Phi_K \times 10^{-12}$	0.10674051	0.10674051[c]	0.10674051[c]
$\phi_J \times 10^{-12}$	0.01087419	0.01087419[c]	0.01087419[c]
$\phi_{JK} \times 10^{-12}$	0.18346025	0.18346025[c]	0.18346025[c]
$\phi_K \times 10^{-12}$	3.06545403	3.06545403[c]	3.06545403[c]
ξ^c		0.2275 (13)	
$\eta^{ab} \times 10^{-4}$		−1.10 (7)	
J_{max}	–	98	72
$K_{a\ max}$	–	46	45
Number trans.	–	4622	2874
rms deviation (cm^{-1})	–		0.000425
σ_{dev}	–		1.0630

[a] Ground state constants from [6].
[b] Figures in brackets are one S.D. according to the least squares fit in units of the least significant figure quoted.
[c] The sextic constants have been constrained to their ground state values.

corresponding to $\zeta^{a} < 0.01$ with no positive effect on the quality of the fit. It should also be noted that evidence was found for a local resonance affecting a few J levels within each K_a stack of ν_2. The perturbing levels are higher in energy at low J, but crossover around $J = 70$ for the $^{q}P_3$ series ($J = 79$ for $^{q}P_9$, etc.). This behaviour rules out ν_7, but suggests that an A′ combination band $\nu_5 + 2\nu_9$ is responsible. Its calculated band centre is 1328 cm^{-1}, and by analogy with ν_6/ν_9 [6] is affected by a strong c-axis Coriolis interaction ζ^{c}_{69} with $\nu_5 + \nu_6 + \nu_9$ which contributes to the required depression in energy as J increases. Because it was not feasible to comprehensively treat such an interaction, the few affected transitions were omitted from the fits.

3.2. $CH^{37}ClF_2$

Because the R22 sample is in natural isotopic abundance, the ratio of $CH^{37}ClF_2$ to $CH^{35}ClF_2$ is 1:3. As a result, the dense spectra dominated by lines from the latter make it difficult to assign the same number of series for $CH^{37}ClF_2$. Many lines are blended, or simply hidden beneath more prominent peaks. It is possible, however, to assign K_a series on the same Loomis–Wood plot used for the other isotopomer, as shown in Fig. 2. Ab initio molecular orbital calculations were performed using Gaussian98 [19] to ascertain approximate ^{37}Cl–^{35}Cl isotopic shifts for the ν_2 and ν_7 band centres, to facilitate and check the correct assignment of J values. The calculated shifts at the HF/6-31G(d) and B3LYP/6-311+G(d,p) levels, respectively, are −0.097 and −0.102 cm^{-1} for ν_2 and −0.016 and −0.015 cm^{-1} for ν_7. The observed shifts of −0.197 and −0.021 cm^{-1} reflect a similar trend. Again a combination of cooled spectra and room temperature spectra were used, and despite the degree of spectral congestion, transitions spanning a good range of quantum numbers were assigned; a total of 1039 lines for ν_2 ($J \leqslant 93, K_a \leqslant 12$) and 682 for ν_7 ($J \leqslant 54, K_a \leqslant 32$). A list of assigned transitions is available from the authors by e-mail.

Individual fits to the two bands yielded the effective constants given in Table 3. The sextic

Table 3
Effective rotational constants in Watson's A-reduced Hamiltonian for ν_2 and ν_7 states of $CH^{37}ClF_2$

Constant	Ground state[a]	ν_2	ν_7
Band centre		1312.894051 (47)[b]	1351.681426 (121)
A	0.341364817	0.34097310 (330)	0.34103977 (85)
B	0.157347146	0.15721474 (62)	0.15726607 (122)
C	0.114474126	0.11317607 (6)	0.11570246 (39)
$\Delta_J \times 10^{-6}$	0.049588272	0.030665 (451)	0.06836 (75)
$\Delta_{JK} \times 10^{-6}$	0.148145488	0.034273 (2263)	0.03260 (178)
$\Delta_K \times 10^{-6}$	0.171658755	1.07703 (9297)	0.26226 (247)
$\delta_J \times 10^{-6}$	0.013769993	0.022464 (226)	0.002827 (435)
$\delta_K \times 10^{-6}$	0.162488411	−0.00689 (1082)	0.20683 (240)
$\Phi_J \times 10^{-12}$	0.0216642	0.3259 (108)	0.5173 (2141)
$\Phi_{JK} \times 10^{-12}$	0.3471063	0.3471063[c]	0.3471063[c]
$\Phi_{KJ} \times 10^{-12}$	−0.1035720	1392.03 (18 741)	−0.1035720[c]
$\Phi_K \times 10^{-12}$	0.1741206	4116.38 (60 203)	−0.0373 (118)
$\phi_J \times 10^{-12}$	0.0101703	0.6982 (59)	−0.5727 (1262)
$\phi_{JK} \times 10^{-12}$	0.1870627	0.1870627[c]	0.1870627[c]
$\phi_K \times 10^{-12}$	3.1481772	−656.437 (93 478)	43.272 (4428)
J_{max}	–	93	54
$K_{a\,max}$	–	12	32
Number trans.	–	1039	682
rms deviation (cm^{-1})	–	0.000994	0.000353
σ_{dev}	–	2.485	0.882

[a] Ground state constants from [7].
[b] Figures in brackets are one S.D. according to the least squares fit in units of the least significant figure quoted.
[c] The sextic constants have been constrained to their ground state values.

Table 4
Rotational constants in Watson's A-reduced Hamiltonian for v_2 and v_7 states of $CH^{37}ClF_2$ incorporating a *c*-axis Coriolis interaction, with ξ^c both fitted and fixed (cm^{-1})

Constant	Ground state[a]	v_2		v_7
Band centre		1312.896189 (38)[b]		1351.681206 (69)
A	0.341364817	0.34091690 (186)		0.34104927 (30)
B	0.157347146	0.15722461 (31)		0.15725645 (47)
C	0.114474126	0.11444445 (4)		0.11442692 (13)
$\Delta_J \times 10^{-6}$	0.049588272	0.04973 (34)		0.04920 (31)
$\Delta_{JK} \times 10^{-6}$	0.148145488	0.11584 (656)		0.15192 (123)
$\Delta_K \times 10^{-6}$	0.171658755	0.26678 (1540)		0.16662 (100)
$\delta_J \times 10^{-6}$	0.013769993	0.01435 (17)		0.01301 (15)
$\delta_K \times 10^{-6}$	0.162488411	0.15197 (198)		0.15472 (193)
$\Phi_J \times 10^{-12}$	0.0216642	0.0216642[c]		0.0216642[c]
$\Phi_{JK} \times 10^{-12}$	0.3471063	0.3471063[c]		0.3471063[c]
$\Phi_{KJ} \times 10^{-12}$	0.1035720	0.1035720[c]		0.1035720[c]
$\Phi_K \times 10^{-12}$	0.1741206	0.1741206[c]		0.1741206[c]
$\phi_J \times 10^{-12}$	0.0101703	0.0101703[c]		0.0101703[c]
$\phi_{JK} \times 10^{-12}$	0.1870627	0.1870627[c]		0.1870627[c]
$\phi_K \times 10^{-12}$	3.1481772	3.1481772[c]		3.1481772[c]
ξ^c			0.2225[d]	
$\eta^{ab} \times 10^{-4}$			−1.0673[d]	
J_{max}		93		54
$K_{a\ max}$		12		32
Number trans.		1039		682
rms deviation (cm^{-1})				0.000392
σ_{dev}				0.979

[a] Ground state constants from [7].
[b] Figures in brackets are one S.D. according to the least squares fit in units of the least significant figure quoted.
[c] The sextic constants have been constrained to their ground state values.
[d] Fixed. See text.

constant were again poorly determined and highly correlated, in this case so much so that Φ_{JK} and ϕ_{JK} (and Φ_{KJ} for v_7) needed to be constrained to the ground state values for the fit to minimise. As an effective set of constants, those in Table 3 are able to reproduce the wavenumber values of fitted transitions, but clearly predictions of further transitions will be poor.

A global fit incorporating the first- and second-order *c*-axis terms revealed a first-order constant, ξ^c, of similar magnitude to $CH^{35}ClF_2$, however η^{ab} was both two orders of magnitude smaller than expected, and poorly determined. It was therefore constrained to a value obtained by multiplying the $^{35}\eta^{ab}$ figure by the appropriate $^{37}A^{37}B/^{35}A^{35}B$ ratio. Additionally, v_2 and v_7 sextic centrifugal distortion constants were constrained to ground state values. The resultant fit was of high quality with an rms error of 0.00040 cm^{-1}. The first-order term ξ^c was fitted to low uncertainty, but the value obtained corresponds to $\zeta^c = 1.004$, marginally exceeding the allowed threshold of 1. A second fit was therefore performed in which ξ^c was fixed at 0.2225, corresponding to the $\zeta^c = 0.971$ value from the $CH^{35}ClF_2$ fit. The results of the latter fit are presented in Table 4.

4. Discussion and conclusions

Simulations of both the cooled and room temperature spectra were performed to test the quality of the constants derived in the fits. The aim was to see how well the constants could reproduce spectral features and to establish the rotational temperature and the a/c-hybrid polarization ratio. A program called SPCAT, written by Pickett [18], was used to predict line positions and intensities and these were convolved with a Gaussian lineshape (FWHH = 0.0025 cm^{-1}). v_7 was simulated

for the purpose of estimating the experimental temperature of the cooled spectra using the shape of the band contour as a guide. This band was used in preference to v_2 due to the unknown nature of the polarisation ratio (μ_a^2/μ_c^2) for the a/c-hybrid band. The rotational temperature was determined to be 180 ± 10 K. The complete simulated and experimental contours are compared in Fig. 1(b) and (c). An expanded section, presented in Fig. 3, shows that the simulation reproduces the line positions and intensities very well.

The inherent width of a- and c-type contours meant that the weaker c-type transitions of v_2 were most clearly discernible on the outskirts of the warmer spectrum. Room temperature simulations were therefore used to determine the polarisation ratio of the a/c-hybrid band. The best match to the observed intensities occurred for an a/c ratio of 5.76 ± 0.5. Fig. 4 shows the simulated and experimental spectra at 296 K for v_2 identifying a- and c-type lines. While Fig. 3 (the v_7 band at 180 K) shows excellent agreement, the comparison in Fig. 4 is not so favourable. Additional features in the room temperature spectrum are attributed to the presence of hot band transitions for both isotopomers, which have not been taken into consideration with the generation of simulated spectra. At 296 K, the Boltzmann populations of v_6 at 413 cm^{-1} and v_9 at 366 cm^{-1} are 13% and 17% of the ground vibrational state. The equivalent populations at 180 K are only 4% and 5%.

A number of parameters obtained through the analysis of the v_2 and v_7 bands may be compared with those predicted from the anharmonic force field of Palmieri et al. [8]. For example, the predicted a/c polarization ratio for v_2, 7.0, is not far from the observed ratio of 5.76 ± 0.5. The ratio of the IR intensity for v_2/v_7 was predicted to be 3.7, whereas a value of 5.6 ± 0.3 was derived from the present analysis. Vibration–rotation interaction constants α were also computed from the anharmonic force field [8]. These incorporate Coriolis resonant contributions, and are therefore directly comparable with the effective constants of Table 1. Table 5 shows that the predictions are useful indicators of the experimental values, lying within about 20% of them. A similar level of agreement is found for the other fundamentals of R22, with the exception of the v_1 CH stretch which is apparently perturbed by Coriolis resonance with a dark state [9].

Given that this work now completes the high-resolution analysis of the nine infrared bands of $CHClF_2$, values for all the vibration–rotation in-

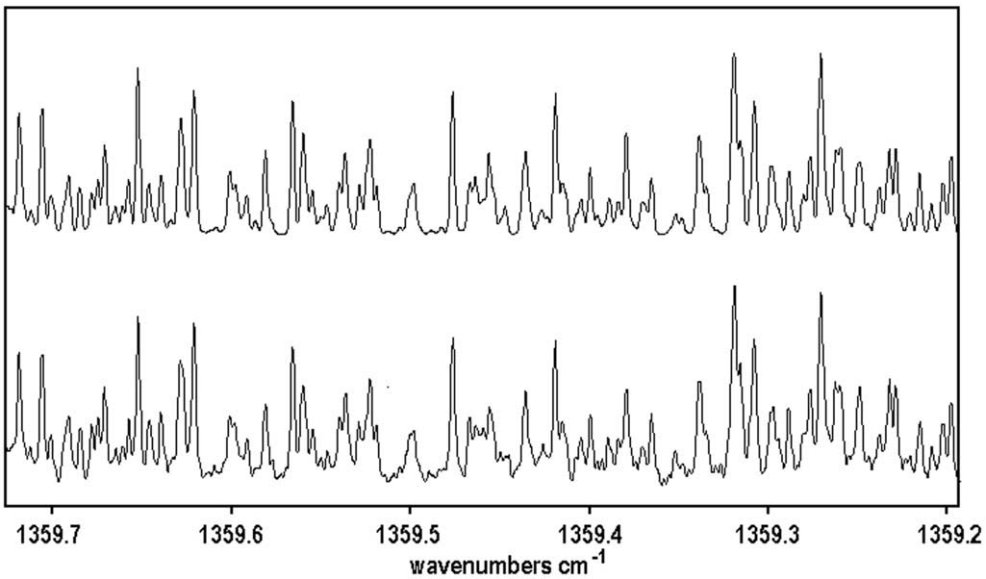

Fig. 3. Expanded section of the 180 K simulation (upper) and cooled experimental (lower) spectrum of the v_7 band of $CHClF_2$.

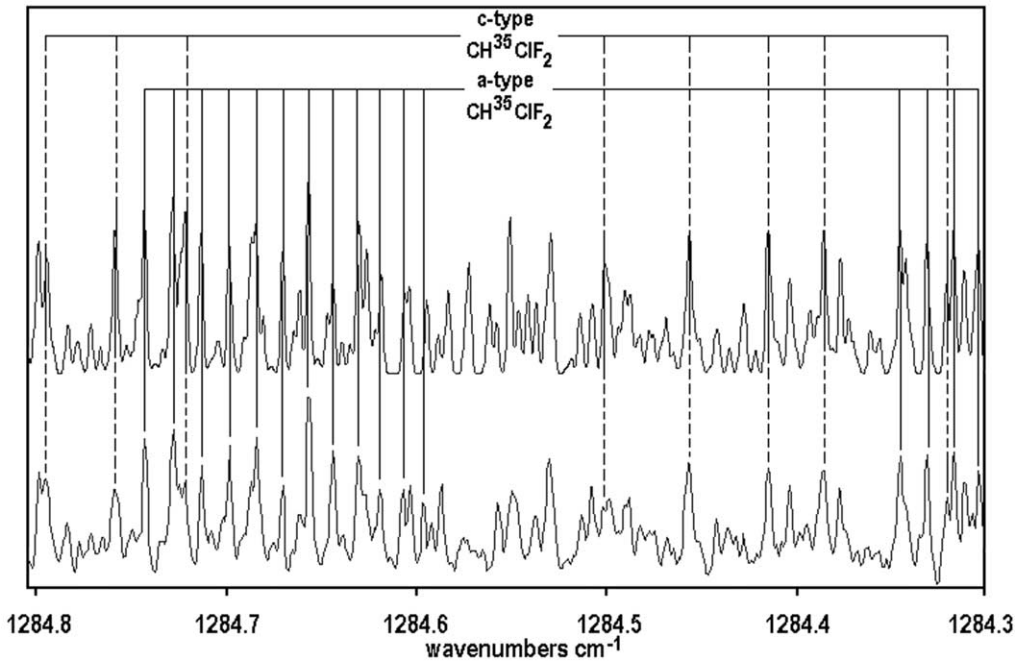

Fig. 4. Simulated (upper) and experimental (lower) spectrum of ν_2 at 296 K showing assigned a- and c-type lines of $CH^{35}ClF_2$.

Table 5
Effective vibration–rotation interaction constants α (cm^{-1}) for $CH^{35}ClF_2$ derived from the data in Table 1 (exp.), compared to those calculated from the anharmonic force field of Palmieri et al. [8] (calc.)

Constant ($\times 10^{-3}$ cm^{-1})	ν_2		ν_7	
	Exp.	Calc.	Exp.	Calc.
α_A	0.450	0.538	0.324	0.241
α_B	0.127	0.103	0.085	0.110
α_C	1.357	1.112	−1.287	−1.055

teraction constants α are known.The equillibrium rotational constants A_e, B_e and C_e can now be calculated in principle – they are 10093.104, 4819.149, 3452.977 MHz, respectively. However, these values must be regarded as approximate only, given the discrepancy between experimental and computed values of α^A, α^B and α^C for ν_1.

Analysis of both cooled and room temperature spectra proved to be an effective means of assigning transitions with a large range of quantum numbers J and K. The degree of spectral simplification provided using the collisional cooling technique was sufficient in that most of the individual rovibrational transitions were resolved. The benefit stems from both fewer rotational levels being populated, and crucially, the virtual disappearance of hot band transitions due to vibrational cooling. Access to transitions of low J, K permitted firm initial assignments to be made. Due to the decreased breadth in the rotational envelope however, lines became indistinguishable from noise as J increased beyond 50 or 60. With higher S/N in this region, the room temperature spectrum provided complementary data. It permitted the assignment of higher J transitions, while congestion made assignment of lines with $J < 30$ impractical. Also, the c-type lines of ν_2 did not emerge beyond the scope of the cooled a-type rotational envelope,

and were discernable only from the room temperature spectra. With fits of the cool data only, some of the centrifugal distortion and Coriolis terms were poorly determined and removed from their expected values. Inclusion of lines assigned from both spectra led to superior results.

Acknowledgements

The authors gratefully acknowledge financial support from the Australian Research Council and a Monash University Logan Fellowship (EGR).

References

[1] United Nations Environment Programme. The 1987 Montreal Protocol on Substances that Deplete the Ozone Layer (Last amended 1999).
[2] Climate Change 1994: Radiative forcing of climate, University Press, Cambridge, 1995.
[3] R. Zander, E. Mahieu, Ph. Demoulin, C.P. Rinsland, D.K. Weisenstein, M.K.W. Ko, N.D. Sze, M.R. Gunson, J. Atmos. Chem. 18 (1994) 129.
[4] D.T. Cramb, Y. Bos, H.M. Jensen, J. Mol. Struct. 190 (1988) 387.
[5] G. Cazzoli, G. Cotti, C.D. Esposti, J. Mol. Spectrosc. 159 (1993) 127.
[6] S. Blanco, A. Lesarri, J.C. Lopez, J.L. Alonso, A. Guarnieri, Z. Naturforsch. A 51 (1996) 129.
[7] Z. Kisiel, J.L. Alonso, S. Blanco, G. Cazzoli, J.M. Colmont, G. Cotti, G. Graner, J.C. Lopez, I. Merke, L. Pszczolkowski, J. Mol. Spectrosc. 184 (1997) 150.
[8] P. Palmieri, R. Tarroni, M.M. Huhn, N.C. Handy, A. Willetts, Chem. Phys. 190 (1995) 327.
[9] G.T. Fraser, J. Domenech, M.-L. Junttila, A.S. Pine, J. Mol. Spectrosc. 152 (1992) 307.
[10] D. Luckhaus, M. Quack, Mol. Phys. 68 (1989) 745.
[11] A. Brown, D.C. McKean, J.L. Duncan, Spectrochim. Acta A 44 (1988) 553.
[12] A. Gambi, P. Stoppa, S. Giorgianni, A. De Lorenzi, R. Visinoni, S. Ghersetti, J. Mol. Spectrosc. 145 (1991) 29.
[13] G. Klatt, G. Graner, S. Klee, G. Mellau, Z. Kisiel, L. Pszczolkowski, J.L. Alonso, J.C. Lopez, J. Mol. Spectrosc. 178 (1996) 108.
[14] I. Merke, G. Graner, S. Glee, O. Polanz, J. Mol. Spectrosc. 173 (1995) 463.
[15] S. Bauerecker, F. Taucher, C. Weitkamp, H.K. Cammenga, J. Mol. Struct. 348 (1995) 237.
[16] D. Appadoo, E.G. Robertson, D. McNaughton, J. Mol. Spectrosc. (submitted).
[17] D. McNaughton, D. McGilvery, F. Shanks, J. Mol. Spectrosc. 149 (1991) 458.
[18] H.M. Pickett, J. Mol. Spectrosc. 148 (1991) 371.
[19] M.J. Frisch et al., Gaussian98, Revision A.6, Gaussian, Inc., Pittsburgh, PA, 1998.